

1<sup>st</sup> International Conference of the Greek Society of Experimental Mechanics of Materials

## Corrosion behavior of 304L stainless steel concrete reinforcement in acid rain using fly ash as corrosion inhibitor

S. Tsouli<sup>a</sup>, A.G. Lekatou<sup>a,\*</sup>, S. Kleftakis<sup>a</sup>, T.E. Matikas<sup>b</sup>, P.T. Dalla<sup>b</sup>

<sup>a</sup>Laboratory of Applied Metallurgy, Department of Materials Science & Engineering, University of Ioannina, Ioannina 45110, Greece

<sup>b</sup>Mechanics, Smart Sensors & Nondestructive Evaluation Laboratory, Department of Materials Science & Engineering, University of Ioannina, Ioannina 45110, Greece

### Abstract

The corrosion performance of 304L stainless steel rebars in a solution simulating concrete exposed to acid rain with the addition of fly ash was studied by means of cyclic potentiodynamic polarization. Fly ash (0-25 wt.%) was added to a concrete simulating solution. 304L rebars embedded in standard concrete cubes containing 0-25 wt.% fly ash were subjected to salt spray testing for 4 m. Tensile testing of the rebars was conducted before and after 2 m of salt spraying. Although 304L showed susceptibility to localized corrosion, the positive effect of fly ash on the corrosion behavior is clearly manifested. Fly ash content of 20 wt.% in the electrolyte led to the highest corrosion resistance. Two months of salt spraying did not affect the tensile behavior of the steel.

© 2018 The Authors. Published by Elsevier Ltd.

This is an open access article under the CC BY-NC-ND license (<http://creativecommons.org/licenses/by-nc-nd/3.0/>)

Peer-review under responsibility of the scientific committee of the 1st International Conference of the Greek Society of Experimental Mechanics of Materials.

**Keywords:** 304L stainless steel rebars; reinforced concrete; fly ash; acid rain; cyclic polarization; salt spray test; tensile test

### 1. Introduction

The ancient monuments of Greece are masterpieces of the world's architectural heritage with immense artistic and historical value. Nowadays modern materials, such as AISI type 316L stainless steel and titanium, are widely employed in restoration works. For example, 316L stainless steel is currently used as reinforcement of ancient archi-

\* Corresponding author. Tel.: +30 26510 07309; fax: +30 26510 07034.

E-mail address: [alekatou@cc.uoi.gr](mailto:alekatou@cc.uoi.gr)

Received: May 04, 2018; Received in revised form: July 18, 2018; Accepted: July 27, 2018

tectural members in the ancient theater of Dodona in Greece. However, as many historical buildings and structures are located in urban and coastal regions, and often in the vicinity of industrial areas, they are subjected to deterioration of the reinforced concrete (Apostolopoulos et al. (2013); Rakanta et al. (2013)).

304L austenitic stainless steel finds many applications, as it combines good corrosion resistance, good mechanical properties and formability. Its good corrosion behavior is owing to the chromia-based passive film on the surface of the steel, as well as the film stabilizing action of nickel (Lekatou (2013); Nagarajan et al. (2007)).

Concrete is nowadays the most predominant material used for the construction of the load bearing elements of structures. This is due to the fact that it is economical, versatile and compatible with the environment, exhibits high mechanical properties, long lifetime often exceeding 100 years, as well as durability against corrosion (Blanco et al. (2006); Mahdikhani et al. (2018)). Concrete is commonly reinforced with steel for mechanical property improvement, as its tensile strength is low. In concrete structures, a passive oxide film is often formed around the concrete reinforcing steel bars (rebars), as a result of the  $\text{Ca}(\text{OH})_2$ -due high alkaline environment ( $\text{pH} \approx 12.5\text{--}13.5$ ); hence, the embedded steel is protected from corrosion (Apostolopoulos et al. (2016); Fan et al. (2010); Monticelli et al. (2016); Sharifi-Asl et al. (2015)).

Although reinforced concrete performs exceptionally well during its service life, the rapid deterioration of the construction service life and seismic resistance has become a growing problem in the last decades. The corrosion of the steel reinforcement is the main factor for the concrete deterioration. This is due to either chloride penetration into the concrete through its pore structure (causing a decrease in the pH), or concrete carbonation (by reaction between atmospheric  $\text{CO}_2$  and  $\text{Ca}(\text{OH})_2$ ). Both processes lead to depassivation and localized corrosion. As a consequence of localized corrosion and rust/corrosion products deposition, internal stresses appear and the concrete around the rebars cracks and spalls (Apostolopoulos et al. (2016); Sharifi-Asl et al. (2015); Zhu et al. (2014)). Corrosion affects both the appearance of the concrete and the bond strength between steel and concrete (Apostolopoulos et al. (2013)). Corrosion of the embedded steel by chloride mostly shows up in coastal areas, whilst carbonation shows up mainly in urban areas (Apostolopoulos et al. (2013; 2016); Zafeiropoulou et al. (2013)).

Over the past twenty years, the acid rain-due pollution has drawn great attention, as the urban and industrial activities have profoundly been increased (Fan et al. (2010)). Acid rain is a strongly corrosive medium, not only containing  $\text{H}^+$ , but also  $\text{NH}_4^+$ ,  $\text{Mg}^{2+}$ ,  $\text{SO}_4^{2-}$ ,  $\text{NO}_3^-$ ,  $\text{Cl}^-$ , etc., thus, causing serious damage on the surface of concrete structures. When reinforced concrete is exposed to an acidic environment, physical and chemical reactions occur causing gradual mass loss and mechanical strength loss, cracking and eventually structural failure (Fan et al. (2010); Wang et al. (2017); Zeng et al. (2018)). Normally, the acid rain-due degradation is a slow process lasting for over several centuries. However, in the last decades it has strongly been accelerated, especially in big cities, near plants, airports etc, causing a severe deterioration in the durability and aesthetical value of architectures (Camuffo (2014)).

Despite the high resistance of stainless steel to corrosion, an excellent localized corrosion behavior is a prerequisite when dealing with cultural heritage in environmentally stressed regions, such as saline, urban, industrial, near airports. Access of aggressive ions being present in these environments, like  $\text{Cl}^-$ ,  $\text{SO}_4^{2-}$ ,  $\text{HCO}_3^-$ ,  $\text{CO}_3^{2-}$ , etc., to the steel surface through the concrete may induce severe localized corrosion. Many famous monuments, including The Acropolis of Athens in Greece and the Statue of Liberty in the USA, have been severely damaged by acid rain in the past decades. Major repairs/replacements become necessary, inducing expensive and inconvenient for the community procedures (Fan et al. (2010); Livingston (2016)).

Nowadays, various methods have been developed to prevent the corrosion of steel reinforcement in polluted environments, such as corrosion inhibitors, galvanization, epoxy coatings, re-alkalization of carbonated concrete, cathodic protection, electrochemical chloride extraction etc. (Chousidis et al. (2015); Chousidis et al. (2016); Criado et al. (2016); Rakanta et al. (2013); Zacharopoulou et al. (2014); Zafeiropoulou et al. (2013)). An often-used corrosion inhibitor is fly ash (FA). Fly ash is a solid, powdery, pozzolanic and non-toxic material formed (as a by-product) by the combustion of pulverized solid fuels (coal, lignite, peat) in the boilers of the thermoelectric power generating plants. When FA is mixed with Portland cement and water, it generates a product similar to that formed by cement hydration, though less permeable (Nath and Sarker (2011)). FA has been shown to positively affect concrete hydration, whilst reducing its porosity, the diffusion of chlorides and  $\text{CO}_2$ , as well as  $\text{CO}_2$  emissions (Chousidis et al. (2016); Nath and Sarker (2011); Uysal and Akyuncu (2012)). Moreover, the FA addition to cement reportedly improves the workability and durability of concrete (by reducing its permeability), reduces the hydration heat and benefits the long-term compressive strength (Hefni et al. (2018); Lu et al. (2018); Nath and Sarker (2011)).

The present study deals with the electrochemical performance of AISI-type 304L rebars immersed in a solution simulating concrete exposed to acid rain. FA has been added as a corrosion inhibitor to the concrete simulating solution. Moreover, the mechanical performance of 304L rebars embedded in FA-containing concrete, before and after salt spray testing, has been examined. The motivation behind this work is the limited literature on the corrosion of concrete-embedded rebars in acid rain, as far as ancient monument restorations are concerned.

### Nomenclature

$E_{\text{corr}}$	corrosion potential
$E_{\text{a/c tr}}$	anodic-to-cathodic transition potential
$i_{\text{corr}}$	corrosion current density
$\sigma_y 0.2\%$	yield strength at 0.2% EL
$\sigma_f$	fracture strength
%EL	elongation

## 2. Experimental protocol

The materials used in this investigation were: rebars of 304L (nominal composition in wt.%: 0.03 C, 18.00 Cr, 8.00 Ni, 1.00 Si, 2.00 Mn, 0.0045 P, 0.03 S) and 316L (nominal composition in wt.%: 0.022 C, 17.31 Cr, 10.08 Ni, 2.02 Mo, 0.54 Si, 1.75 Mn, 0.0032 P, 0.0001 S) stainless steels of 6 mm diameter and 2.5 cm length; 304L rebars embedded in concrete cubes ( $7^3 \text{ cm}^3$ ) and fly ash from the Hellenic Public Power Corporation lignite mines in Western Macedonia. Previous work (Tsouli et al. (2018)) has shown that the FA is composed by (in decreasing order of concentration) CaO, SiO<sub>2</sub>, Al<sub>2</sub>O<sub>3</sub>, SO<sub>3</sub>, Fe<sub>2</sub>O<sub>3</sub> (minor amounts) and MgO (minor amounts).

Potentiodynamic polarization tests (4 replicate runs for each specimen) were conducted on 304L rebars, the cut edges of which had been mounted in epoxy resin (three electrode cell, Ag/AgCl/3.5 M KCl, Pt, 4 h immersion under open circuit to reach steady state, room temperature, 10 mV/min scan rate, ACM-Gill AC potentiostat/galvanostat). A series of polarization runs was performed on 316L, as well, for comparison reasons. The corrosion current densities were calculated by Tafel extrapolation, adopting several restrictions analytically reported in previous works (Lekatou et al. (2012); Lekatou et al. (2015)). The susceptibility of the steels to localized corrosion was investigated by cyclic polarization. The main concept of this technique is that pitting would occur if the current density of the anodic portion of the return scan is higher than the current density of the forward scan for the same anodic potential (“negative” hysteresis) (Lekatou et al. (2015)). A naturally aerated aqueous saturated (s.) Ca(OH)<sub>2</sub> solution containing an acid rain simulating solution and different FA contents was employed as an electrolyte. The s. Ca(OH)<sub>2</sub> solution simulates concrete pore environments (Blanco et al. (2006); Volpi et al. (2015)). The chemical analysis of the acid rain simulating solution (pH=3.1) was (g/l water): H<sub>2</sub>SO<sub>4</sub>: 0.032, HNO<sub>3</sub>: 0.015, Na<sub>2</sub>SO<sub>4</sub>: 0.032, NaNO<sub>3</sub>: 0.021, NaCl: 0.084, (NH<sub>4</sub>)<sub>2</sub>SO<sub>4</sub>: 0.046. After the necessary metallographic preparation, the microstructure of the specimens (cross-sectioned at ribs) was examined by SEM (Scanning Electron Microscopy)/EDX (Energy Dispersion X-ray spectroscopy) (Jeol JSM 6510 LV SEM / Oxford Instruments X- Act EDX).

304L rebars embedded in standard concrete cubes were subjected to salt spray testing for 4 m (Vötsch Ind. GmbH, ASTM B117-97). Tensile testing of the rebars (3 replicate runs for each specimen) was conducted before and after 2 m of salt spraying (Galdabini, 100 kN, ASTM E8/E8M-09).

## 3. Results and discussion

### 3.1. Cyclic potentiodynamic polarization

Representative cyclic polarization curves of 304L rebars during immersion in s. Ca(OH)<sub>2</sub> containing acid rain simulating solution and different FA contents are presented in Fig. 1a. Critical electrochemical values extracted from the polarization curves are listed in Table 1. Fig. 1b also includes forward polarization curves of 316L rebars immersed in the same electrolyte, for comparison reasons.

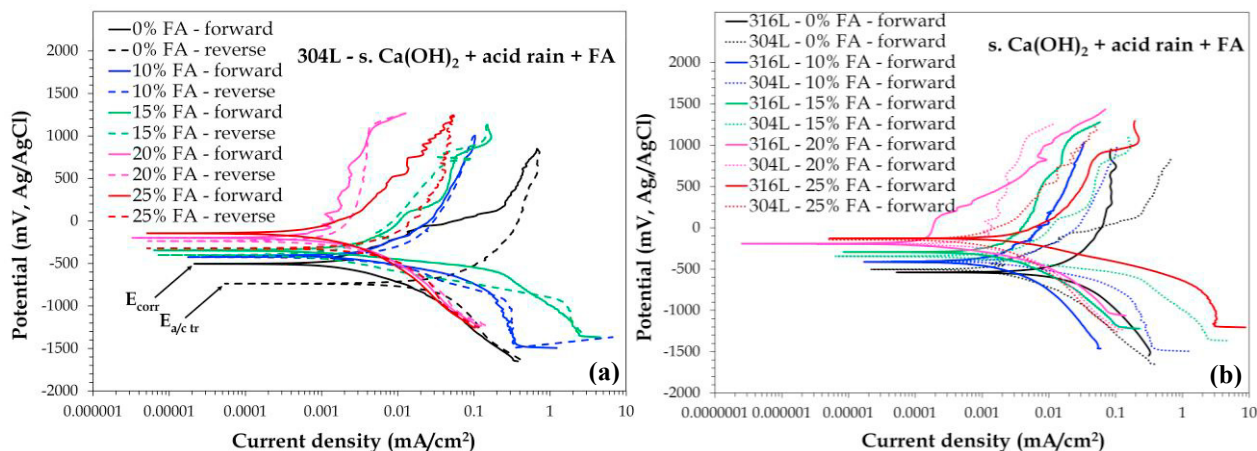


Fig. 1. (a) Cyclic voltammograms of 304L rebar in s.  $\text{Ca}(\text{OH})_2$  containing acid rain simulating solution and different fly ash (FA) contents; (b) Comparison of the polarization behaviors of 316L and 304L rebar in the same electrolyte.

Table 1. Electrochemical values of 304L stainless steel rebar immersed in s.  $\text{Ca}(\text{OH})_2$  containing acid rain simulating solution and fly ash.

Fly ash (wt.%)	$E_{\text{corr}}$ (mV, Ag/AgCl)	$E_{\text{a/c tr}}$ (mV, Ag/AgCl)	$i_{\text{corr}}$ (mA/cm <sup>2</sup> )
0	-481±93	-583±114	0.0024±0.0001
10	-489±52	-378±73	0.0019±0.0001
15	-448±102	-345±89	0.0018±0.0001
20	-381±141	-277±51	0.0017±0.0001
25	-281±122	-295±125	0.0021±0.0001

The negative hysteresis loops of the anodic polarization curves (i.e. higher current densities upon reverse polarization as compared to the forward polarization for the same potential) in the majority of the polarization curves (Fig.1a), show that 304L has been subjected to localized corrosion. Nevertheless, as seen in Table 1, in all cases except those of 0 and 25 wt.% FA, the  $E_{\text{a/c tr}}$  values are higher than or nearly equal to the  $E_{\text{corr}}$  values, indicating nobler or equally noble surfaces at  $E_{\text{a/c tr}}$  (reverse polarization) than or to those at  $E_{\text{corr}}$  (forward polarization). Fig. 1a shows that the negative hysteresis loops at 0 and 25 wt.% FA present large surface areas, indicating significant localized corrosion. All forward anodic polarization curves except that of 0 wt.% FA exhibit regimes of drastic current density reduction; moreover, the current limiting currents are lower than 0.1 mA/cm<sup>2</sup> indicating surface films of high resistivity.

Table 1 shows that the FA addition has generally led to less thermodynamic tendency for corrosion (nobler  $E_{\text{corr}}$ ), which is attributed to the increase in the pH of the electrolyte with FA content increasing (Table 2), according to the well-known Nernst equation (Lekatou (2013)):

$$E = E^{\circ} + 0.0059 \text{ pH} \quad (1)$$

where  $E$  is the equilibrium potential of the galvanic cell and  $E^{\circ}$  is the equilibrium potential of the galvanic cell under standard conditions. The increase in the pH values with time shown in Table 2, indicates a hydration reaction of the type (Nath and Sarker (2011)):



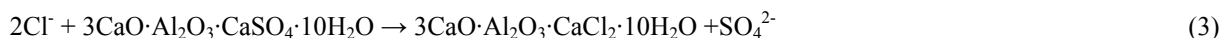
that releases  $\text{OH}^-$  into the electrolyte. The higher the amount of FA in the electrolyte the higher the  $\text{OH}^-$  concentration, thus justifying the pH increase with FA addition (Table 2).

Fig. 1a manifests that addition of FA to the electrolyte (up to 20 wt.%) has led to a shift of the forward polarization curves to lower currents and a higher resistance to localized corrosion (negative hysteresis loops of small surface area or even positive hysteresis loops). Table 1 reveals a decrease in  $i_{\text{corr}}$  (i.e. uniform corrosion rate) with FA addition up to 20 wt.%. The superiority of the corrosion behavior corresponding to the 20 wt.% FA content, as far as corrosion kinetics is concerned, is evident in both Fig. 1a and Table 1 (lowest currents, best defined passive regime and lowest  $i_{\text{corr}}$ ). However, the trend of corrosion resistance increasing with FA content is reversed at 25 wt.% FA. Not only is the hysteresis negative but the hysteresis loop has a large surface area. In addition, a small but noticeable increase in  $i_{\text{corr}}$  over that corresponding to 20 wt.% FA is observed in Table 1.

Table 2. pH values of 304L rebars at the end of the open circuit state and cathodic polarization in s. Ca(OH)<sub>2</sub> containing acid rain and fly ash.

Fly ash (wt.%)	pH (0 h)	pH (4 h-open circuit)	pH (6 h - E <sub>corr</sub> )
0	4.50	5.00	5.50
10	5.50	6.00	6.50
15	6.00	6.50	7.00
20	6.50	7.00	7.50
25	6.90	7.40	7.90

The positive effect of FA on the corrosion performance of the reinforced concrete has frequently been reported in literature. The pozzolanic reaction between FA and Ca(OH)<sub>2</sub> leads to the formation of calcium silicate hydrates, thereby decreasing the hydration heat release and drying shrinkage of the reinforced concrete and improving the pore structure of the concrete (Chousidis et al. (2016); Moffat et al. (2017); Yue et al. (2018)). In the present case, it is postulated that the interaction of FA with Ca(OH)<sub>2</sub> has led to the formation of mixed hydrated salts of complex formulae (most likely including 3CaO·Al<sub>2</sub>O<sub>3</sub> and 4CaO·Al<sub>2</sub>O<sub>3</sub>·Fe<sub>2</sub>O<sub>3</sub>) on the steel surface. These salts may trap Cl<sup>-</sup> by chemical and/or physical bonding, thereby delaying and/or limiting the aggressive Cl<sup>-</sup> access to the steel. The above consideration is compatible with the formation of the Friedel's salt (calcium chloroaluminate) in FA containing cement (Chousidis et al. (2016); Jiayu et al. (2014); Yue et al. (2018)):



The deterioration in the electrochemical performance at the 25 wt.% FA content can be explained by the agglomeration of FA particles that has resulted in a non-uniform distribution along the surface of the steel specimens. Interaction of the agglomerates with Ca(OH)<sub>2</sub> may have produced deposits on the surface of the steel of large surface area, that can lead to “deposit corrosion”, as will be discussed in section 3.2.

Comparison of the voltammograms of 304L with those of 316L rebars (Fig. 1b), manifests higher corrosion resistance of 316L rebars as compared to 304L rebars, in terms of slower corrosion kinetics (shift of polarization curves to lower currents) and less thermodynamic tendency for corrosion (nobler E<sub>corr</sub>). The 316L rebars also exhibit a high resistance to localized corrosion, as previously shown (Tsouli et al. (2018)). The superiority of the corrosion performance of 316L rebar over that of 304L rebar is mainly attributed to the presence of Mo in 316L, the higher content of Ni in 316L and the lower content of S in 316L. Mo improves the resistance to localized corrosion in chloride containing environments. Sulfur in the form of sulfides promotes pit corrosion. Ni promotes the stabilization of the passive film (Lekatou (2013)).

In both cases, the addition of FA to the electrolyte has led to a shift of the forward polarization curves to lower currents suggesting slower corrosion kinetics. For both steels, the superiority of the corrosion behavior corresponding to the 20 wt.% FA, as far as corrosion kinetics is concerned, is evident. However, even the addition of 10 wt.% or 15 wt.% FA to the electrolyte (304L rebars) has led to slower corrosion kinetics and higher resistance to localized corrosion (positive or zero hysteresis loops) compared to 316L in the FA free electrolyte. Hence, it is suggested that 304L can replace 316L in the restoration of ancient monuments provided that fly ash is employed as a corrosion inhibitor.

### 3.2. Microstructure of corroded specimens

This section attempts to explain the deterioration of the corrosion performance of the 304L rebars in the 25 wt.% FA electrolyte (Figs.2a-d). First of all, Fig.2a demonstrates the beneficial role of FA addition, as it has locally formed a compact film on steel inhibiting  $\text{Cl}^-$  penetration into the steel (arrow-pointed in Fig. 2a). A typical EDX spectrum from this film in Fig. 2b reveals that the film is the product of the FA (Ca, Si, Al, S, Mg, K) and steel (Fe, Cr, Ni) interaction. The detection of noticeable amounts of Cl and S (besides Ca, Si, Al and O) constitutes evidence of a composition analogous to the reaction product of equation (3). Fig.2c presents the destructive role of FA at high FA additions. Pits and surface film seem to be associated with high FA amounts in the following way: FA (through the reaction with  $\text{Ca}(\text{OH})_2$  and  $\text{Cl}^-$ ) has locally formed a thick deposit on the steel surface. As a consequence, differential aeration cells are formed, where the steel below a relatively compact part of the deposit (reduced  $\text{pO}_2$ ) acts as an anode and the steel below a less dense part of the deposit (higher  $\text{pO}_2$ ) acts as a cathode. The anode corrodes forming pits filled with corrosion products (from FA- $\text{Ca}(\text{OH})_2$ -acid rain-steel interactions).

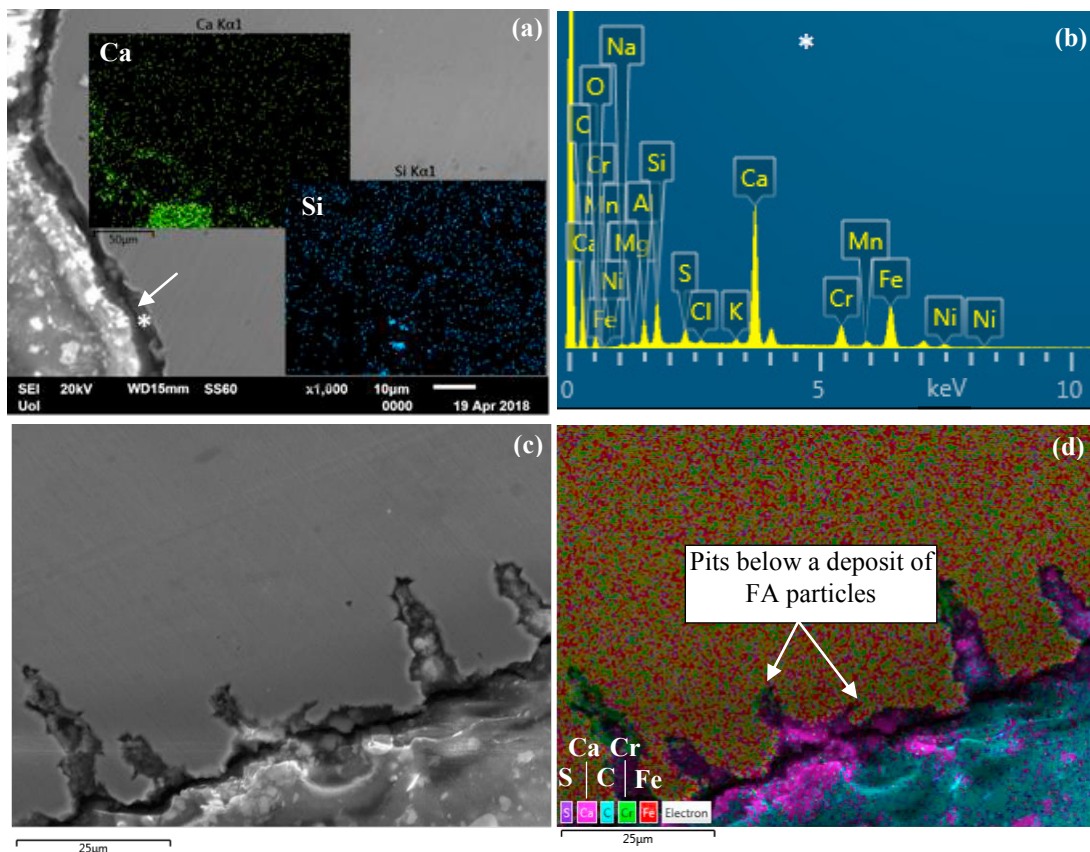


Fig. 2. SEM micrographs of 304L rebar after cyclic polarization in s.  $\text{Ca}(\text{OH})_2$  containing acid rain simulating solution and 25 wt.% FA. (a) A compact film on the steel surface (arrow-pointed); inset: EDX mapping for Ca and Si; (b) Representative point EDX spectrum from the compact film in (a); (c) Pitting below agglomerates of FA particles; (d) EDX mapping of (c): purple: S, magenta: Ca; turquoise: C; green: Cr, red: Fe.

### 3.3. Salt spray and tensile tests

Figs.3(a,b) presents the macrostructural state of a 304L reinforced concrete cube (20 wt.% FA) after exposure into the salt spray chamber for 4 m. The fine state of the specimen is obvious. Most important, Fig.3c and Table 3 show that salt spraying for 2 m did not affect the tensile properties of the 304L rebars embedded in the concrete.

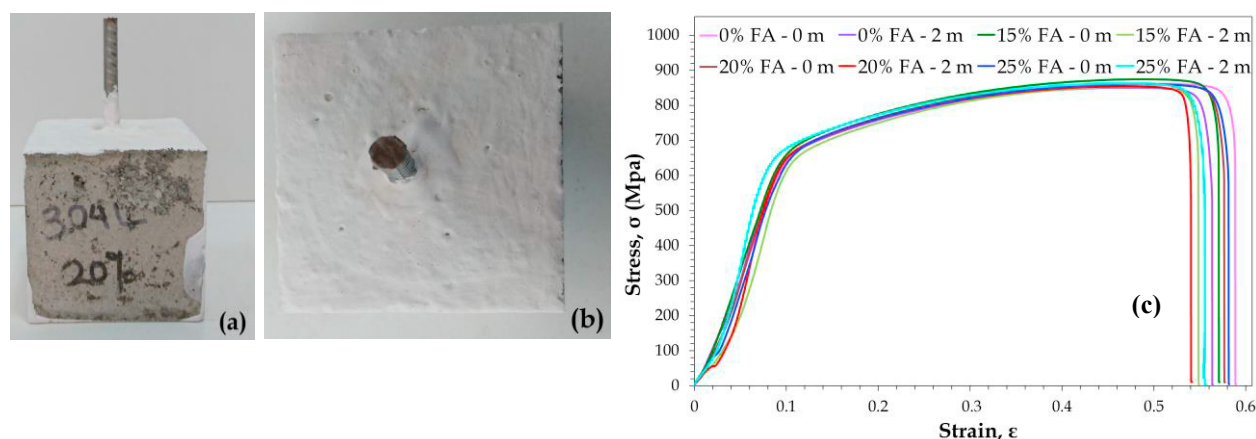


Fig. 3. 304L reinforced concrete after 4 m in the salt spray chamber: (a) Side-view; (b) Top-view of 304L reinforced concrete containing 20 wt.% FA; (c) Stress-strain curves of 304L rebars embedded in concrete with different fly ash (FA) contents before (0 m) and after salt spraying (2 m).

Table 3. Tensile properties of 304L rebars embedded in concrete with different fly ash contents before (0 m) and after salt spraying (2 m).

Fly ash (wt.%)	Duration (m)	$\sigma_y$ , 0.2% (MPa)	$\sigma_t$ (MPa)	$\sigma_r$ (MPa)	% EL
0	0	611±31	782±31	726±50	44±0
	2	605±50	776±58	720±57	42±1
15	0	619±30	790±27	732±3	43±1
	2	555±44	729±52	667±24	41±2
20	0	586±15	754±16	686±20	43±1
	2	594±19	771±18	735±4	40±2
25	0	592±8	753±11	669±1	42±1
	2	598±41	780±38	706±31	43±0

#### 4. Conclusions

Cyclic polarization of 304L stainless steel rebars in s. Ca(OH)<sub>2</sub> containing an acid rain simulating solution and different fly ash (FA) amounts revealed slow corrosion kinetics, passive-like regimes and low susceptibility to localized corrosion (10-20 wt.% FA). An increase in the FA addition led to a decrease in the thermodynamic tendency for corrosion and corrosion kinetics. This trend was reversed at 25 wt.% FA. Corrosion-wise, 304L can replace 316L stainless steel in the restoration of ancient monuments provided that FA is included in the concrete mixture as a corrosion inhibitor, even at low contents (10 or 15 wt.%). Salt spraying for 2 m did not affect the mechanical properties of the 304L rebars embedded in concrete cubes. Not any macrostructural signs of corrosion were observed in 304L reinforced concrete cubes after a 4 m salt spray test.

#### References

- Apostolopoulos, Ch.A., Demis, S., Papadakis, V.G., 2013. Chloride-induced corrosion of steel reinforcement - Mechanical performance and pit depth analysis. *Construction and Building Materials* 38, 139-146.
- Apostolopoulos, A., Matikas, Th.E., 2016. Corrosion of bare and embedded in concrete steel bar – Impact on mechanical behavior. *International Journal of Structural Integrity* 7, 240-259.
- Blanco, G., Bautista, A., Takenouti, H., 2006. EIS study of passivation of austenitic and duplex stainless steels reinforcements in simulated pore solutions. *Cement & Concrete Composites* 28, 212-219.
- Camuffo, D., 2014. Atmospheric Water and Stone Weathering, in “*Microclimate for Cultural Heritage. Conservation, Restoration, and Maintenance of Indoor and Outdoor Monuments*”. 2<sup>nd</sup> Ed., Elsevier Science, pp. 203-243.
- Chousidis, N., Ioannou, I., Rakanta, E., Koutsodontis, C., Batis, G., 2016. Effect of fly ash chemical composition on the reinforcement corrosion, thermal diffusion and strength of blended cement concretes. *Construction and Building Materials* 126, 86-97.

- Chousidis, N., Rakanta, E., Ioannou, I., Batis, G., 2015. Anticorrosive effect of electrochemical manganese dioxide by-products in reinforced concrete. *Journal of Materials Science and Chemical Engineering* 3, 9-20.
- Criado, M., Sobrados, I., Bastidas, J.M., Sanz J., 2016. Corrosion behaviour of coated steel rebars in carbonated and chloride-contaminated alkali-activated fly ash mortar. *Progress in Organic Coatings* 99, 11-22.
- Fan, Y.F., Hu, Z.Q., Zhang, Y.Z., Liu, J.L., 2010. Deterioration of compressive property of concrete under simulated acid rain environment. *Construction and Building Materials* 24, 1975-1983.
- Hefni, Y., Abd El Zaher, Y., Abdel Wahab, M., 2018. Influence of activation of fly ash on the mechanical properties of concrete. *Construction and Building Materials* 172, 728-734.
- Jiayu, M., Zhibao, L., Yuehua, J., Xiaoping, Y., 2014. Synthesis, characterization and formation mechanism of friedel's salt (FS:  $3\text{CaO}\cdot\text{Al}_2\text{O}_3\cdot\text{CaCl}_2\cdot 10\text{H}_2\text{O}$ ) by the reaction of calcium chloride with sodium aluminate. *Journal of Wuhan University of Technology - Materials Science Edition* 30, 76-83.
- Lekatou, A., 2013. *"Corrosion and Protection of Metals in Simple Words"*. Nemertes Publications, Athens, ISBN: 978-960-9951-2-4.
- Lekatou, A., Sfikas, A.K., Karantzalis, A.E., Sioulas, D., 2012. Microstructure and corrosion performance of Al-32%Co alloys. *Corrosion Science* 63, 193-209.
- Lekatou, A., Sioulas, D., Karantzalis, A.E., Grimanelis, D., 2015. A comparative study on the microstructure and surface property evaluation of coatings produced from nanostructured and conventional WC-Co powders HVOF-sprayed on Al 7075. *Surface and Coatings Technology* 276, 539-556.
- Livingston, R.A., 2016. Acid rain attack on outdoor sculpture in perspective. *Atmospheric Environment* 146, 332-345.
- Lu, C., Wang, W., Li, Q., Hao, M., Xu, Y., 2018. Effects of micro-environmental climate on the carbonation depth and the ph value in fly ash concrete. *Journal of Cleaner Production* 181, 309-317.
- Mahdikhani, M., Bamshad, O., Fallah Shirvani, M., 2018. Mechanical properties and durability of concrete specimens containing nano silica in sulfuric acid rain condition. *Construction and Building Materials* 167, 929-935.
- Moffatt, E.G., Moffatt, M.D.A., Fahim, A., 2017. Performance of high-volume fly ash concrete in marine environment. *Cement and Concrete Research* 102, 127-135.
- Monticelli, C., Natali, M.E., Balbo, A., Chiavari, C., Zanotto, F., Manzi, S., Bignozzi, M.C., 2016. Corrosion behavior of steel in alkali-activated fly ash mortars in the light of their microstructural, mechanical and chemical characterization. *Cement and Concrete Research* 80, 60-68.
- Nagarajan, S., Karthega, M., Rajendran, N., 2007. Pitting corrosion studies of super austenitic stainless steels in natural sea water using dynamic electrochemical impedance spectroscopy. *Journal of Applied Electrochemistry* 37, 195-201.
- Nath, P., Sarker, P., 2011. Effect of fly ash on the durability properties of high strength concrete. *Procedia Engineering* 14, 1149-1156.
- Rakanta, E., Zafeiropoulou, Th., Batis, G., 2013. Corrosion protection of steel with DMEA-based organic inhibitor. *Construction and Building Materials* 44, 507-513.
- Sharifi-Asl, S., Mao, F., Lu, P., Kursten, B., Macdonald, D.D., 2015. Exploration of the effect of chloride ion concentration and temperature on pitting corrosion of carbon steel in saturated  $\text{Ca}(\text{OH})_2$  solution. *Corrosion Science* 98, 708-715.
- Tsouli, S., Lekatou, A.G., Kleftakis S., 2018. The Effect of Fly Ash on the Corrosion Performance of AISI 316L Stainless Steel Reinforced Concrete for Application to Restoration Works of Ancient Monuments, in *"10th International Symposium on the Conservation of Monuments in the Mediterranean Basin. Natural and Anthropogenic Hazards and Sustainable Preservation"*. Springer Nature, Chapter 17, ISBN: 978-3-319-78092-4.
- Uysal, M., Akyuncu, V., 2012. Durability Performance of concrete incorporating class F and class C fly ashes. *Construction and Building Materials* 34, 170-178.
- Volpi, E., Olietti, A., Stefanoni, M., Trasatti, S.P., 2015. Electrochemical characterization of mild steel in alkaline solutions simulating concrete environment. *Journal of Electroanalytical Chemistry* 736, 38-46.
- Wang, P., Zhu, Z., Sun, X., Wang, X., 2017. Deterioration of fracture toughness of concrete under acid rain environment. *Engineering Failure Analysis* 77, 76-84.
- Yue, Y., Wang, J.J., Muhammed Basheer, P.A., Bai, Y., 2018. Raman spectroscopic investigation of friedel's salt. *Cement and Concrete Composites* 86, 306-314.
- Zacharopoulou, A., Zacharopoulou, E., Batis, G., 2014. Protection systems for reinforced concrete with corrosion inhibitors. *Open Journal of Metal* 4, 86-92.
- Zafeiropoulou, Th., Rakanta, E., Batis, G., 2013. Carbonation resistance and anticorrosive properties of organic coatings for concrete structures. *Journal of Surface Engineered Materials and Advanced Technology* 3, 67-74.
- Zeng, X., Li, Y., Ran, Y., Yang, K., Qu, F., Wang, P., 2018. Deterioration mechanism of CA mortar due to simulated acid rain. *Construction and Building Materials Special Issue Railway Engineering-2015* 168, 1008-1015.
- Zhu, H., Zhang, Z., Zhu, Y., Tian, L., 2014. Durability of alkali-activated fly ash concrete: chloride penetration in pastes and mortars. *Construction and Building Materials* 65, 51-59.